MULTILAMINATE ELASTOPLASTIC MODEL FOR GRANULAR MEDIA

S.A. Sadrnezhad
Department of Civil Engineering
Khajeh-Nasirodin Toosi University of Technology
Tehran, Iran

Abstract A multilaminate based model capable of predicting the behavior of granular material on the basis of sliding mechanisms and elastic behavior of particles is presented. The capability of the model to predict the behavior of sand under arbitrary stress paths is examined. The influences of rotation of the direction of principal stress axes and induced anisotropy are included in a rational way without any additional hypotheses. The predicted numerical results of sand specimens in hollow cylindrical and true triaxial tests and also under undrained conditions are presented.

چکیده در این مقاله یک مدل برپایهٔ رفتار مواد دانه ای بصورت صفحات متعدد لغزشی و دانه های ارتجاعی، جهت پیش بینی رفتار این گونه مواد ارائه شده است. قابلیت این مدل در پیشگویی رفتارماسه تحت اعمال مسیرهای تنشی دلخواه آزمایش شده است. آثار چرخش محورهای اصلی تنش و ناهمسانی تحمیلی در حین تغییر شکلهای خمیری بصورتی مناسب در تئوری این مدل بدون فرضیات اضافی نهفته‌اند. نتایج تحلیل عددی رفتار نمونه‌های ماسه در آزمایشات مکعب خاك و سلیندر توخالی در شرایط زهکشی نشده و زهکشی شده ارائه گشته اند.

INTRODUCTION

For a granular mass such as sand that supports overall applied loads through contact friction, the overall mechanical response ideally may be described on the basis of micro-mechanical behavior of grains interconnections. Naturally, this requires the description of overall stress, characterization of fabric, representation of kinematics, development of local rate constitutive relations and evaluation of the overall differential constitutive relations in terms of the local quantities.

The task of representing the overall stress tensor in terms of micro-level stresses and the condition, number and magnitude of contact forces has long been the aim of numerous researchers [1-3].

In recent years, another class of models called 'multilaminate model' was developed by Zienkiewics and Pande [4] for jointed rock masses and by Pande and Sharma [5] for clays. Bazant and Oh [6] have developed a similar model for fracture analysis of concrete under the name 'microplane model'.

An eleastoplastic model, 'reflecting surface model' was developed by Pande and Pietruszczak [7] and used to predict cyclic loading behavior of normally consolidated and lightly over-consolidated clays. Shiomi et al. [8] used this model for the prediction of liquefaction of sand layers.

This paper presents a multilaminate model capable of predicting the behavior of granular material under monotonic, cyclic loading and other respectively complex stress paths.

The concept of the proposed model is natural, physically meaningful and extremely simple. According to this formulation, which is based on a simple numerical integration, an appropriate connection between averaged micro and macro-mechanical behavior of material has been presented. The inclusion of the rotation of principal stress and strain axes, induced anisotropy and the possibility of supervising and even controlling any variation through the medium are the significant features of the model.

BASIC ASSUMPTIONS AND DISCUSSIONS

Multilaminate framework, by defining the small continuum structural units as an assemblage of particles and voids which fill infinite spaces between the sampling planes, has appropriately justified the contribution of interconnection forces in overall macro-mechanics. Plastic deformations are assumed to occur due to sliding, separation/closing of the boundaries; and elastic deformations are the overall responses of structural unit bodies. Therefore, the overall deformation of any small part of the medium is composed of total elastic reponse and an appropriate summation of sliding, separation/closing phenomenon under the current effective normal and shear stresses on sampling planes.

According to these assumptions overall sliding, separation/closing of intergranular points of grains included in

one structural unit are summed up and contributed as the result of sliding, separation/closing surrounding boundary planes. This simply implies yielding/failure or even ill-conditioning and bifurcation response to be possible over any of the randomly oriented sampling planes. Consequently, plasticity control such as yielding should be checked at each of the planes and those of the planes which are sliding will contribute to plastic deformation. Therefore, the granular material mass has an infinite number of yield functions usually one for each of the planes in the physical space.

The Constitutive Equations of Multilaminate Model

The classical decomposition of strain increments under the concept of elasto-plasticity in elastic and plastic parts are schematically written as follows:

$$d\underset{\sim}{\varepsilon} = d\underset{\sim}{\varepsilon}^e + d\underset{\sim}{\varepsilon}^p \qquad (1)$$

The increment of elastic strain ($d\underset{\sim}{\varepsilon}^e$) is related to the increments of effective stress ($d\underset{\sim}{\sigma}$) by :

$$d\underset{\sim}{\varepsilon}^e = \underset{\sim}{C}^e . d\underset{\sim}{\sigma} \qquad (2)$$

where, $\underset{\sim}{C}^e$ is elastic compliance matrix, usually assumed as linear. Conceptually, it is possible to compute $\underset{\sim}{C}^e$ by using the multilaminate framework. However, if the single structural units are assumed to be elastically isotropic, using a common elasticity tensor, then trivially, the overall elastic response of the collective system will be isotropic, having the same elasticity tensor. Clearly, in this case, computing C^e by using multilaminate framework is not fruitful. When single structural unit constituents are anisotropic, then, whether or not the overall elastic response will be isotropic depends on the distribution of the single structural units. For a random distribution, the overall response will be isotropic, whereas this response will be anisotropic if the distribution of particle orientations is biased by prior plastic deformation.

For the soil mass, the overall stress-strain increments relation, to obtain plastic strain increments ($d\underset{\sim}{\varepsilon}^p$), is expressed as:

$$d\underset{\sim}{\varepsilon}^p = \underset{\sim}{C}^p . d\underset{\sim}{\sigma}' \qquad (3)$$

where, $\underset{\sim}{C}^p$ is the plastic compliance matrix.

Clearly, it is expected that all the effects of plastic behavior be included in $\underset{\sim}{C}^p$. To find $\underset{\sim}{C}^p$, the constitutive equations for a typical slip plane must be considered in the calculations. Consequently, the appropriate summation of all provided compliance matrices corresponding to considered slip planes yields overall $\underset{\sim}{C}^p$.

Constitutive Equations for a Sampling Plane

As already defined, plastic strain is calculated from the study of the glide motion over an individual sampling plane. To explain the plasticity constitutive law for a sampling plane, the main features of plasticity law (i.e. yield criterion, plastic potential function, flow rule and hardening rule) must also be considered.

Yield Criterion

In this constitutive formulation, the yield criterion is defined by the ratio of the shear stress (τ_i) to the normal effective stress(σ_{ni}) on i^{th} sampling plane. The simplest form of yield function i.e. a straight line on τ versus σ_n space is adopted. As the ratio τ/σ_n increases, the yield surface represented by the straight line rotates anticlockwise due to hardening and approaches Mohr-Coulomb's failure line and finally failure on the corresponding plane takes place.

The equation of yield function is formulated as follows:

$$F_i(\tau_i, \sigma_{ni}, \eta_i) = \tau_i - \eta_i \sigma_{ni} \qquad (4)$$

where, $\eta_i = \tan(\alpha_i)$ is a hardening parameter and assumed as a hyperbolic function of plastic shear strain on the i^{th} plan. α_i is the slope of yield line.

To provide elastic behavior of cohesionless material at the start of stress increment or whenever the direction of stress path changes, a small elastic domain (defined by angle $\varnothing_e$) is considered. This domain as shown in Figure 1 is small and negligible. Therefore, the value of $\varnothing_e$ for all sands is assumed to be the same. However, the minimum valueof η_i is $\tan(\varnothing_e)$ at the first loading process.

PLASTIC POTENTIAL FUNCTION

Feda [9] derived the plastic potential function which is used in this research.This function is stated in terms of τ_i and σ'_{ni} for the τ versus σ'_n space as follows:

$$\psi(\tau_i, \sigma'_{ni}) = \tau_i + \eta_c . \sigma'_{ni} \log_e(\sigma_{ni}/\sigma_{nio}) \qquad (5)$$

where, η_c is the slope of critical state line and σ'_{ni} is the initial value of effective normal stress on i^{th} plane. Typical presentations of this function are shown in Figure 1. The gradient of this function represents contractant and dilatant behavior in the ranges as:

$$0.0 \le \tau_i \le \sigma'_{ni} . \eta_c \quad \text{(contractant behavior)} \qquad (6)$$

$\tau_i \geq \sigma'_{ni} \eta_c$ (dilatant behavior) (7)

Derivative of this function is found as:

$$\partial\psi_i/\partial\underset{\sim}{\sigma}'_i = \{1.0, \eta_c - \eta_i\}^T \quad (8)$$

Where, η_i is the hardening parameter or the slope of yield line in i^{th} plane.

Obviously, dilatancy is positive if $\eta_i > \eta_c$ and negative if $\eta_i < \eta_c$. On critical state line $\eta_i = \eta_c$ volumetric plastic strain.

Accordingly, the derivatives of the adopted plastic potential function which are based on the conception of energy Equation [10,11], can only be expressed in terms of variable η_i, and identify the components of plastic strain increment ratio as well as the position of no dilatancy/ contractancy on τ versus σ_n space. This aspect seems to be the most suitable form which conforms with the constitutive formulation of sampling plane for granular media.

NON-ASSOCTATED FLOW RULE AND CONSISTENCY CONDITION

Flow rule is expressed as follows:

$$d\underset{\sim}{\varepsilon}_i^p = \lambda_i \frac{d\psi_i}{d\underset{\sim}{\sigma}'_i} \quad (9)$$

Where λ_i is the proportionality scalar parameter and changes during plastic deformations.

In theory of plastic flow, the consistency condition is a necessary condition which requires that a yield criterion be satisfied as far as the material is in a plastic state. Mathematically, this condition is stated as follows:

$$\{\partial F_i/\partial\underset{\sim}{\sigma}'\}^T . d\underset{\sim}{\sigma}' + \partial F_i/\partial k_i . dk_i = 0.0 \quad (10)$$

where in the first loading process $k_i = \varepsilon_i^{pt}$ and ε_i^{pt} is plastic shear strain on the i^{th} plane. Substituting Equation (9) in (10), $d\lambda_i$ is obtained as follows:

$$d\lambda_i = -\frac{\{\partial F_i/\partial\underset{\sim}{\sigma}'_i\}^T . d\underset{\sim}{\sigma}'_i}{\{\partial F_i/\partial k_i\} . \{\partial\psi_i/\partial\tau_i\}} \quad (11)$$

or

$$d\underset{\sim}{\varepsilon}_i^p = -\frac{\{\partial F_i/\partial\underset{\sim}{\sigma}'_i\}^T . d\underset{\sim}{\sigma}' \{\partial\psi_i/\partial\underset{\sim}{\sigma}'\}}{\{\partial F_i/\partial k_i\} . \{\partial\psi_i/\partial k_i\}} \quad (12)$$

This relation can also be expressed in another form as:

$$d\underset{\sim}{\varepsilon}_i^p = \{1/Hp_i\} . \{\partial F_i/\partial\underset{\sim}{\sigma}'_i\}^T . \{\partial\psi_i/\partial\underset{\sim}{\sigma}'\} . d\underset{\sim}{\sigma}'_i \quad (13)$$

where Hp_i is defined as hardening modulus of i^{th} plane and is obtained as follows:

$$Hp_i = -\{\partial F_i/\partial k_i\} . \{\partial\psi_i/\partial\tau_i\} \quad (14)$$

therefore, $$d\underset{\sim}{\varepsilon}_i^p = \underset{\sim}{C}_i^p . d\underset{\sim}{\sigma}' \quad (15)$$

where:

$$\underset{\sim}{C}_i^p = \{1/Hp_i\} \{\partial\psi_i/\partial\sigma'_i\} \{\partial F_i \partial\sigma'_i\}^T$$

$\underset{\sim}{C}_i^p$ as a whole, represents the plastic resistance corresponding to i^{th} plane and must be summed up as the contribution o this plane with the others. Accordingly the conceptua numerical integration of multilaminate frame-work present the following summation for computing $\underset{\sim}{C}^p$.

$$\underset{\sim}{C}^p = 4\Pi . \sum_{i=1}^{n} W_i \underset{\sim i}{\hat{C}^p}$$

where W_i is the weight coefficients and $\underset{\sim}{C}^p$ is the global plastic compliance matrix corresponding to a single point in the medium. A simple function simulates the best variation of this property during the plastic flow which has been represented as a hyperbolic function as follows:

$$\eta_i = \frac{K_i . \tan(\varnothing_f)}{A_i + K_i} \quad (18)$$

where, $K_i = (\varepsilon_i^{pt} - \varepsilon_{oi}^{pt})$, $\varnothing_f$ is the peak internal frictional angle, and A_i is a soil parameter. ε_i^{pt} and ε_{oi}^{pt} are current and initial values of plastic shear strain on i^{th} plane. It must be noted that at first loading ε_{oi}^{pt} is equal to zero and its value is renewed at each change of load increment sign. η_i starts from $\varnothing_e$, grows aaccompanied with the plastic shear strain and slowly approaches the failure line. However, as stated for dense soils, it has to slowly rotate back towards the critical state line.

FIRST LOADING

The behavior of soil is assumed to be elastic in a small zone as shown in Figure 1. This conforms with a small value of η_i which is equal to $\tan(\varnothing_e)$.

A simple form of variation of η_i is a hyperbolic function which has been considered. However, the range of variation of η_i is between - $\tan(\varnothing_f)$ and + $\tan(\varnothing_f)$. The following relation is an equation which is used for first loading.

$$\eta_i = \frac{(\varepsilon_i^{pt} - \varepsilon_{oi}^{pt}) . (m . \tan(\varnothing_f) - \eta_{oi})}{A_i + (\varepsilon_i^{pt} - \varepsilon_{oi}^{pt})} + \eta_{oi} \quad (19)$$

A_i is a material constant and for first loading it is equal to A_o, where A_o is the initial value of this parameter. η_{oi} and ε^{pl}_{oi} are the values of η_i and ε^{pl}_i when the last change in the direction in stress path has taken place. For first loading ε^{pl}_{oi} and η_{oi} are equal to zero. m for first loading is equal to +1. The value A_o is found by trial and error by comparing computer results with experimental results of triaxial compression tests.

UNLOADING

To obtain comparable theoretical and experimental results the value of A must be changed. Another reason for this, is the different shape of hysteresis loop when cyclic loading takes place at different positions. A value obtained from numerical experiments is given by:

$$A_i = A_o + 0.075.\varepsilon^{pl}_{oi} \qquad (20)$$

Equations (19) and (20) are valid for unloading and m must equal -1 for unloading process. Clearly, the value of η_i approaches $-\tan(\varnothing_f)$ while ε^{pl}_i is large enough in comparison to A_i.

RELOADING

The variation of η_i for reloading process is similar to unloading although the limit value of η_i is $+\tan(\varnothing_f)$. m is equal to +1 and the value of A_i must change. The new value of A_i is shown as follows:

$$A_i = (\bar{\varepsilon}^{pl}_{oi} - \varepsilon^{pl}_{oi}).\{(\tan(\varnothing_f) - \eta_{oi})/(\bar{\eta}_{oi} - \eta_{oi}).0\} \qquad (21)$$

where $\bar{\varepsilon}^{pl}_{oi}$ and $\bar{\eta}_{oi}$ are the values of ε^{pl}_{oi} and n_i at the start of unloading process. ε^{pl}_{oi} and η_{oi} are similar values at the start of reloading process.

Finally, this form of the variation for η_i as a unique equation at each process, can produce hysteresis energy loops with different widths. The higher the absolute values of ε^{pl}_{oi} and η_{oi} the higher the width of hysteredsis energy loops produced.

DEFINITION OF PLANES IN THREE DIMENSIONAL MEDIA

To satisfy the conditions of applicability of the theory from the engineering viewpoint and also to reduce the extremely high computational costs, a limited number of necessary and sufficient sampling planes are considered.

As stated in reference [5], the choice of 13 independent planes for the solution of any three dimensional problem is a fair number. The orientation of the sampling planes as given by their direction cosines and the weight coefficients for numerical integration rule are given in Table 1.

TABLE 1.Direction Cosines and Weight Coefficients of Integration Points.

Direction cosines of integration points			Weights
l_i	m_i	n_i	W_i
$+\sqrt{\frac{1}{3}}$	$+\sqrt{\frac{1}{3}}$	$+\sqrt{\frac{1}{3}}$	27/840
$+\sqrt{\frac{1}{3}}$	$-\sqrt{\frac{1}{3}}$	$+\sqrt{\frac{1}{3}}$	27/840
$-\sqrt{\frac{1}{3}}$	$+\sqrt{\frac{1}{3}}$	$+\sqrt{\frac{1}{3}}$	27/840
$-\sqrt{\frac{1}{3}}$	$-\sqrt{\frac{1}{3}}$	$+\sqrt{\frac{1}{3}}$	27/840
$+\sqrt{\frac{1}{2}}$	$+\sqrt{\frac{1}{2}}$	0.0	32/840
$-\sqrt{\frac{1}{2}}$	$+\sqrt{\frac{1}{2}}$	0.0	32/840
$+\sqrt{\frac{1}{2}}$	0.0	$+\sqrt{\frac{1}{2}}$	32/840
$-\sqrt{\frac{1}{2}}$	0.0	$+\sqrt{\frac{1}{2}}$	32/840
0.0	$-\sqrt{\frac{1}{2}}$	$+\sqrt{\frac{1}{2}}$	32/840
0.0	$+\sqrt{\frac{1}{2}}$	$+\sqrt{\frac{1}{2}}$	32/840
1.0	0.0	0.0	40/840
0.0	1.0	0.0	40/840
0.0	0.0	1.0	40/840

Figure 2 shows the orientation of all 13 planes in similar cubes. In order to clarify their positions, they have been presented in four cubes.

IDENTIFICATION OF PARAMETERS

In a general case, for the most anisotropic, non-homogeneous material, 13 sets of material parameters corresponding to plastic sliding of each of the sampling planes are required. However, any knowledge about the similarity of the sliding behavior of different sampling planes reduces the number of required parameters.

The number of parameters required in the proposed model to obtain the behavior of an isotropic homogeneous sand is five. Two of these parameters correspond to elastic behavior of soil skeleton and the rest to plastic flow on each sampling plane. These parameters are listed as follows:

1) Elastic modulus, E
2) Poisson ratio, ν
3) Slope of critical state line, η_c

4) Constant value in hardening function, A_o
5) Peak angle of internal friction, $\varnothing_f$

E and ν are found in the usual way as for any other model. The other three parameters correspond to the plastic behavior of one plane. In this research, these three parameters have been assumed to be the same for all 13 defined planes because of initial isotropic conditions.

In order to calibrate the model, two sets of test results concerning hollow cylindrical and true triaxial tests [12] consisting of monotonic compression and extension and also compression cyclic loading have been considered. The first set of test results consists of five hollow cylindrical tests used to calibrate the model and the other set for verification.

The values of parameters used in computations are shown in Table 2.

TABLE 2. Parameter Values

parameter	value / unit
E'	229.667 MPa.
ϑ	0.377
η_c	$0.800 \times \tan(\varnothing_f)$
A_o	0.0005

The value of $\varnothing_f$ for the tests with initial mean pressure is equal to 203 KPa. Thus $\varnothing_f$ is equal to 37.8° and while $\sigma'_{no} \geq 350$ KPa. is equal to 36.38°.

It must be noted that there is another parameter ($\varnothing_\theta$) which defines the elastic domain. The value of this parameter is small and thus can sometimes be ignored; also it is ineffective to make any change in the overall model results. Therefore, the value of this paramether for all tests even for different sands is equal to 0.57°.

THE MODEL RESPONSE UNDER UNDRAINED CONDITIONS

The principle of effective stress is stated as follows:

$$\underset{\sim}{\sigma} = \underset{\sim}{\sigma'} + \underset{\sim}{m}\, U \qquad (22)$$

where $\underset{\sim}{\sigma}$ and $\underset{\sim}{\sigma'}$ are representative of total and effective stresses vectors, respectively, $\underset{\sim}{m}$ is constant operator vector which is equal to $\{1,1,1,0,0,0\}^T$, and U is excess pore water pressure. This equation can be written in incremental form as:

$$d\underset{\sim}{\sigma} = d\underset{\sim}{\sigma'} + \underset{\sim}{m}\, dU \qquad (23)$$

where d is used for representing small increments.

It can also be assumed that in a fully undrained case, the skeleton volume change is precisely equal to change in the volume of pore water. Equation (22) can be rewritten as:

$$dU = K_f \,.\, \{\underset{\sim}{m}\}^T . d\underset{\sim}{\varepsilon}. \qquad (24)$$

where K_f is obtained [13] as follows:

$$\frac{1}{K_f} = \frac{1}{K_w} + \frac{1-\theta}{K_s} \qquad (25)$$

where K_w bulk modulus of water and θ is initial porosity. Therefore,

$$d\underset{\sim}{U} = K_f \,.\, \{\underset{\sim}{m}\}^T . d\underset{\sim}{\varepsilon} . \{\underset{\sim}{m}\} \qquad (26)$$

Retaining the elastoplastic constitutive law, it is presented as follows:

$$d\underset{\sim}{\sigma'} = \underset{\sim}{D}^{ep} . d\underset{\sim}{\varepsilon}$$

$$d\underset{\sim}{\sigma} = \underset{\sim}{D}^{ept} . d\underset{\sim}{\varepsilon}$$

where $\underset{\sim}{D}^{ep}$ and $\underset{\sim}{D}^{ept}$ are effective and total stress-strain matrices. Substituting Equations (26), (27) and (28) in (23), the result is written as:

$$\underset{\sim}{D}^{ept} = \underset{\sim}{D}^{ep} + K_f \,.\, \{\underset{\sim}{m}\}^T . \{\underset{\sim}{m}\}$$

where

$$\underset{\sim}{D}^{ep} = [\underset{\sim}{C}^{ep}]^{-1}$$

$$\underset{\sim}{D}^{ep} = \underset{\sim}{C}^{e} + \underset{\sim}{C}^{p}$$

where $\underset{\sim}{C}^{e}$, $\underset{\sim}{C}^{p}$, and $\underset{\sim}{C}^{ep}$ are compliance elasticity, plasticity, and elasto-plasticity matrices, respectively.

According to incremental algorithm, $\underset{\sim}{C}^{ep}$ computed in the previous step can be used for the current step; therefore, the solution will not remain indeterminate.

Undrained Triaxial Standard Test

Considering axi-symmetric strain control scheme, the known variables is $d\varepsilon_z$ and unknown variables are dU, and $d\sigma_z$.

Equation (23) can be abbreviated for this case as follows:

$$\begin{bmatrix} d\sigma'_x \\ d\sigma'_y \\ d\sigma'_z \end{bmatrix} = \begin{bmatrix} -dU \\ -dU \\ d\sigma_z - dU \end{bmatrix} = \begin{bmatrix} \\ D^{ep} \\ \\ \end{bmatrix} \cdot \begin{bmatrix} -(1/2)\, d\varepsilon_z \\ -(1/2)\, d\varepsilon_z \\ d\varepsilon_z \end{bmatrix}$$

Similar to strain control scheme, the stress-strain matrix equation is carried out as follows:

$$\begin{bmatrix} -(1/2)\,d\varepsilon_z \\ -(1/2)\,d\varepsilon_z \\ d\varepsilon_z \end{bmatrix} = \begin{bmatrix} C^{ep} \end{bmatrix} \cdot \begin{bmatrix} -dU \\ -dU \\ d\sigma_z - dU \end{bmatrix} \qquad (33)$$

The above matrix equation represents two independent equations. The value of dU simply is a function of $d\varepsilon_z$ and can be obtained from the first or second row, however, substituting this statement in the third row leads the solution to obtain $d\varepsilon_z$. The substitution of this value in either the first or second row and represents dU. In this process, $\underset{\sim}{C}^{ep}$ from the previous step can be used in the computations.

UNDRAINED PREDICTED RESULTS

From the results presented here, it can be concluded that the model reproduces salient features of sand behavior under monotonic loading. The model has shown how boiling in a loose sand (low initial hydrostatic pressures) is produced after pore water pressure built-up leading to failure. This is precisely in agreement with the concept of liquefaction [14] as when pore pressure rises sufficiently to destroy the material strength. It is noted that the same value of $\varnothing_f$ was used for both cases.

CONCLUSION

From this study a model capable of predicting the behavior of granular material on the basis of sliding mechanisms and elastic behavior of particles has been presented. The concept of multilaminate framework was applied successfully for granular materials. However, this is achieved by the use of generally simplified, applicable, effective, and easily understandable relations between micro and macro scales. These relations demonstrate an easy way to handle any heterogeneous material property as well as mechanical behavior of materials. Significantly, the stress-strain relations are primarily defined on the sampling planes, therefore there is no need to handle tonsorial invariance requirements which are a source of great difficulty in constitutive modeling. In this way, not only the tonsorial invariance is subsequently ensured, but some more effects which, in ordinary models are missed, are additionally included. This inclusion is achieved by combining the responses from sampling planes of all orientations within the material. Consequently, these results are a step closer to real plastic behavior of soil.

This model is able to solve a three dimensional plasticity problem by a rather simple theory based on the phenomenological description of two dimensional plastic deformation and kinematic hardening of materials. This actually, is achieved in such a way that the application of some difficult tasks such as induced anisotropy and rotation of principal stress and strain axes which take place during plastic flow, are out of constitutive relations. Accordingly, the sampling plane constitutive formulations provide convenient means to classify loading events, generate history rules and formulate independent evolution rules for local variables.

The behavior of soil has also been modeled based on a semi-microscopic concept which is very close to the reality of particle movement in soils.

Kinematic and isotropic hardening based phenomenological features on sampling planes are contributed and appropriately summed up, therefore, the solution of any complexities involved in random cyclic loading can be obtained and presented.

In spite of producing the final results in macro scale, there is another significant feature that represents the ability of being informed of the semi-micro scales procedures during any transient monotonic or cyclic loading stress path. This feature is very beneficial in clarifying the history and rate of all local average microscales variations through the medium. The final thing which can be gained through this process is the information about failure and corresponding orientation through the medium.

REFERENCES

1. M. M. Christofferson, Mehrabadi and S Nemat-Nasser, *J. Appl. Mech.*, 48, 339-344 (1981).
2. J. Konishi, Proc. U.S. -Japan Seminar on Continuum-Mechanical and Statistical Approaches in the Mechanics of Granular Materials (Eds. S. C. Cowin and M. Satake), pp. 27-45, Gakujutsu Bunken Fukyukai, Tokyo, (1978).
3. S. Nemat-Nasser and M.M. Mehrabadi "Stress and Fabric in Granular Masses, Mechanics of Granular Materials;" New Models and Constitutive Relations (Eds. J.T. Jenkins and M. Satake), pp. 1-8, Elsevier Sci. Pub. (1983).
4. O.C. Zienkiewicz, and G.N. Pande, *J. Num. Anal. Methods in Geomechanics* 1, 219-247, (1977).
5. G.N. Pande and K.G. Sharma, *Int. J. for Numerical and Analyt. Meth. in Geomech.* (1983)
6. Z.P. Bazant and B.H. Oh. Microplane model for fracture analysis of concrete structures, Proceeding Symposium on the Interaction of Non-nuclear Munitions with Structures, held at US Air Force Academy, Colorado Springs, Published by McGregor & Werner, Washington DC (1983).
7. G.N. Pande and S. Pietruszczak Proceeding International Symposium Numerical Methods in Geomechanics, Zurich, A.A. Balkema, Roterdom, 50-64, (1982).
8. T. Shiomi S. Pietruszczak, and G.N. Pande, Proceeding International Symposium Numerical Methods in Geomechanics, Zurich, Balkema, Roterdom, 411-418, (1982).
9. J. Feda,Proc. First Bulg. Nat, Cong. Theor. Appl. Mech. Varna,

Sofia, vol. 1, 387-399 (1971).
10. D.W. Taylor, Fundamentals of Soil Mechanics, J. Wiley & Sons, 2nd reprint 700, (1966).
11. A.W. Bishop, *Geotechnique*, 2(1), 113-116 (1950).
12- International workshop on constitutive equations for granular non-cohesive soils, Information Package Case Western Uni. Cleveland, July 22-24, (1987).
13. D.J. Naylor, G.N., Pande, B. Simpson, and R. Tabb. Finite Elements in Geotechnical Engineering, Pineridge Press, Swansea, (1983).
14. A. Casagrande, Liquefaction and Cyclic Deformation of Sand- A critical review, 5th Pan American Conference on Soil Mechanics and Foundation Engineering, Buenos Aires, Argentina, (1975).
15. S.A. Sadrnezhad and G.N. Pande. A multilaminate model for sands, Proceeding of 3rd International Symposium on Numerical Models in Geomechanics, NUMOG III, held on 8-11 May, Niagara Falls, Canada (1989).

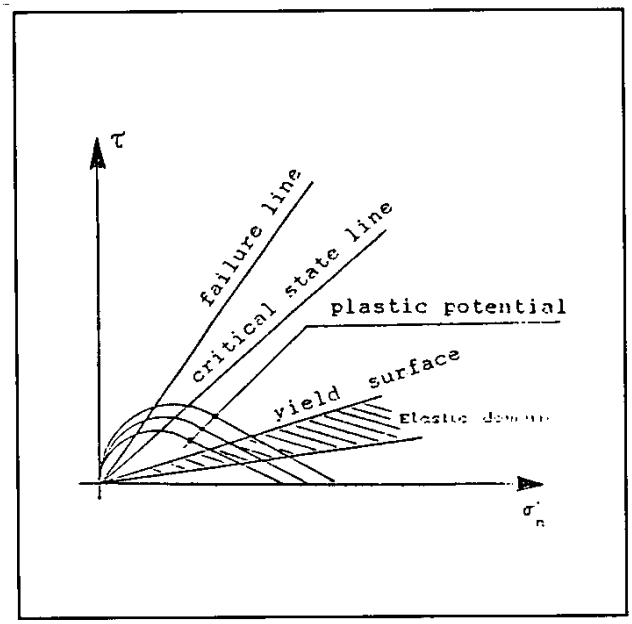

Figure. 1. Yield criterion, plastic potential, elastic zone, critical state line, and failure line in τ - σ_n space.

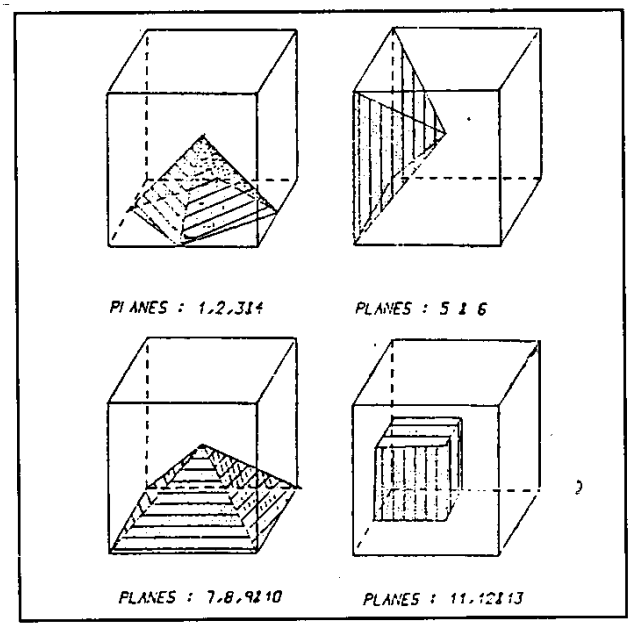

Figure. 2. Demonstration of the orientation of 13 planes.

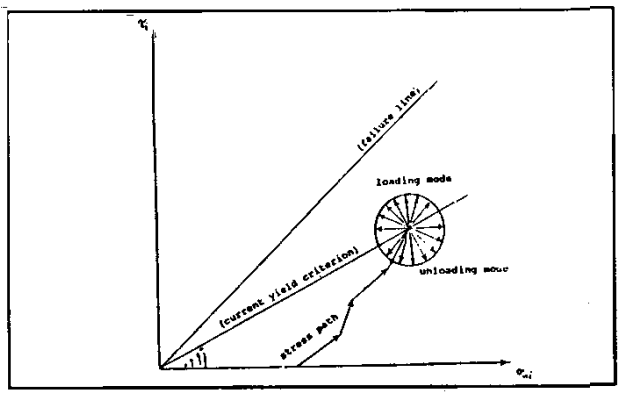

Figure. 3. Loading and unloading modes with respest to the current position of yield surface.

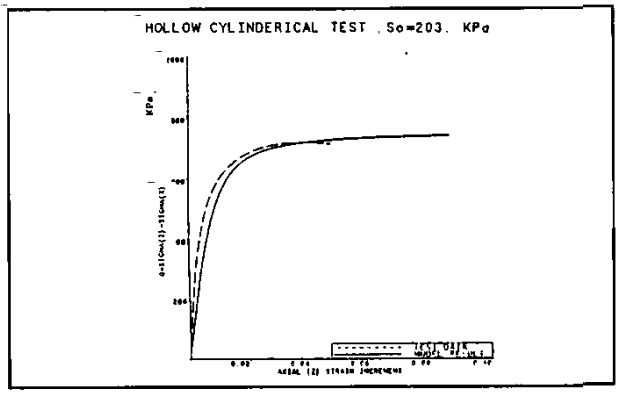

a) Stress deviator (Q) versus axial strain (ε_z)

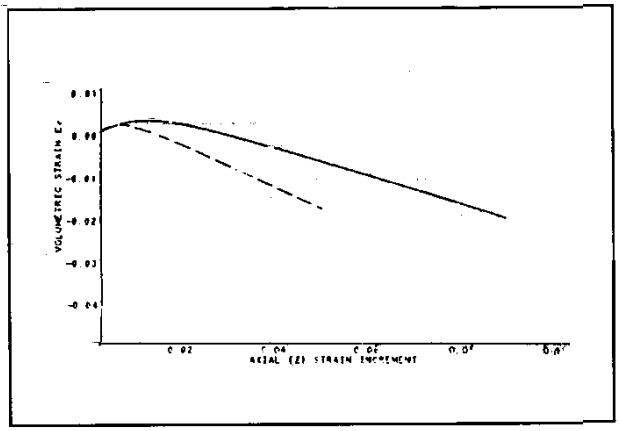

b) Volumetric strain (ε_v)versus axial strain (ε_z)

Figure. 4. The comparison of model response with HH1. TST

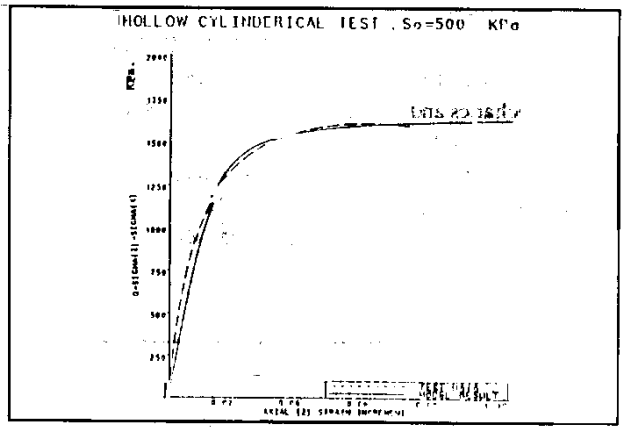

a) Stress deviator (Q) versus axial strain (ε_z)

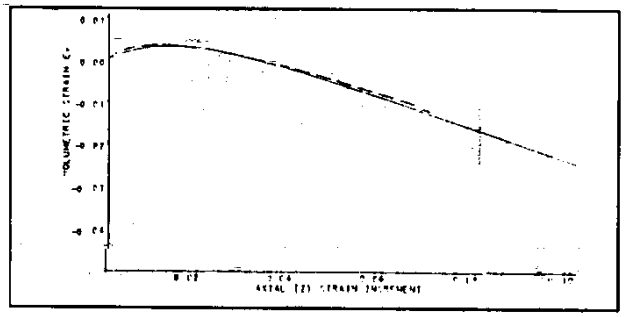

b) Volumetric strain (ε_v) versus axial strain (ε_z)

Figure. 5. The comparison of model response with HH2. TST

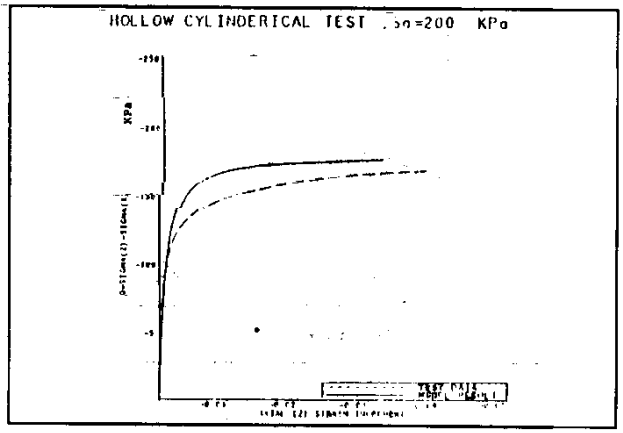

a) Stress deviator (Q) versus axial strain (ε_z).

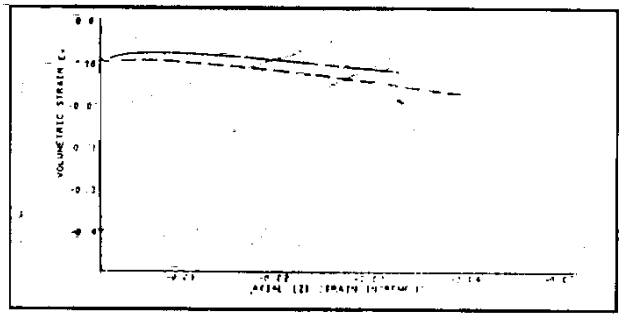

b) Volumetric strain (ε_v) versus axial strain (ε_z).

Figure. 6. The comparison of model response with HH3. TST

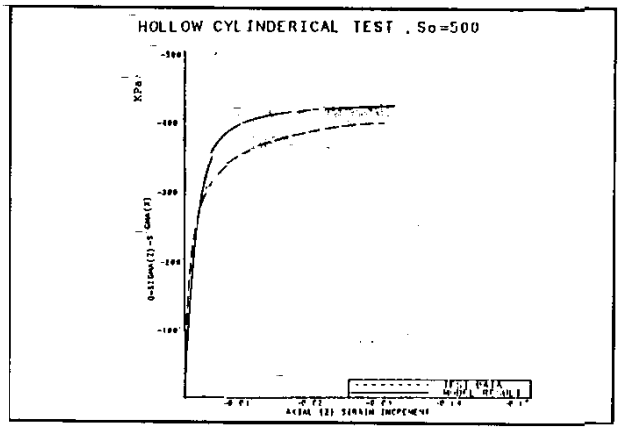

a) Stress deviator (Q) versus axial strain (ε_z)

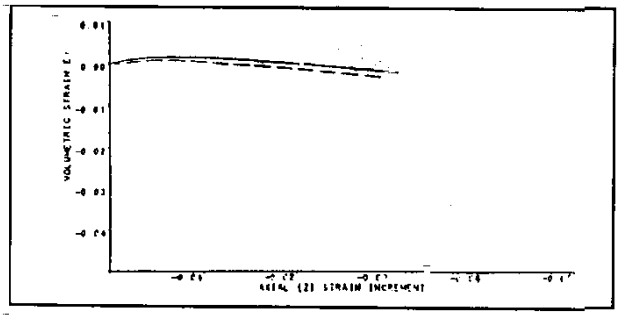

b) Volumetric strain (ε_v) versus axial strain (ε_z)

Figure. 7. The comparison of model response with HH4. TST

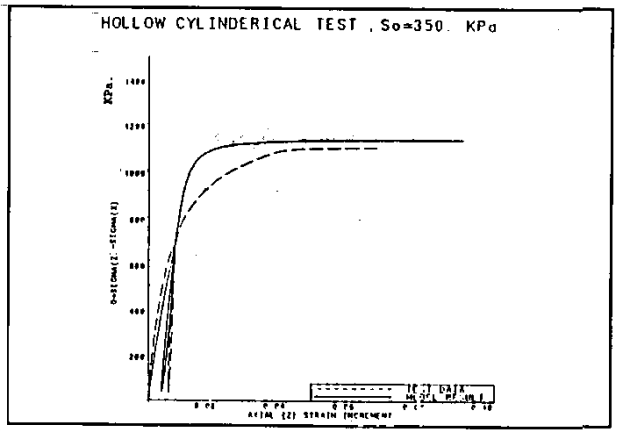

a) Stress deviator (Q) versus axial strain (ε_z).

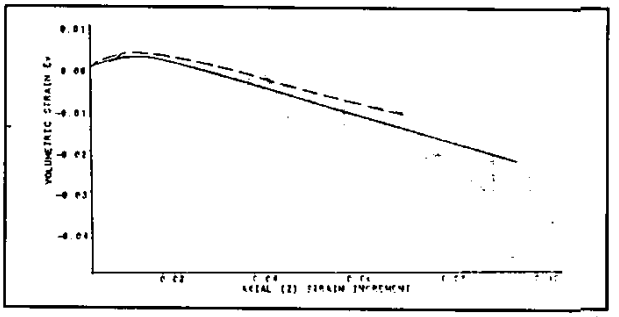

b) Volumetric strain (ε_v) versus axial strain (ε_z)

Figure. 8. The comparison of model response with HH5. TST

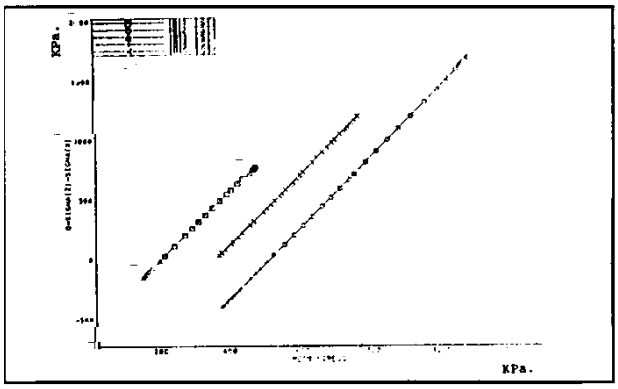

Figure. 9. Total stress paths for tests HH1. TST, HH2. TST, HH3. TST, HH4. TST and HH5. TST

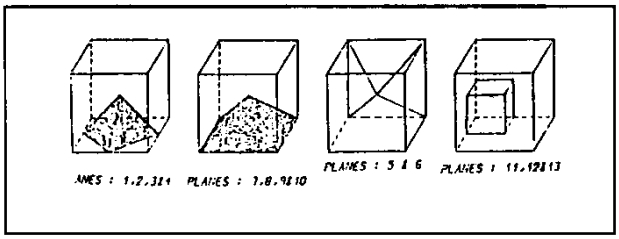

Figure. 10. Active planes in tests: HH1. TST, HH2. TST, HH3. TST, HH4. TST and HH5. TST

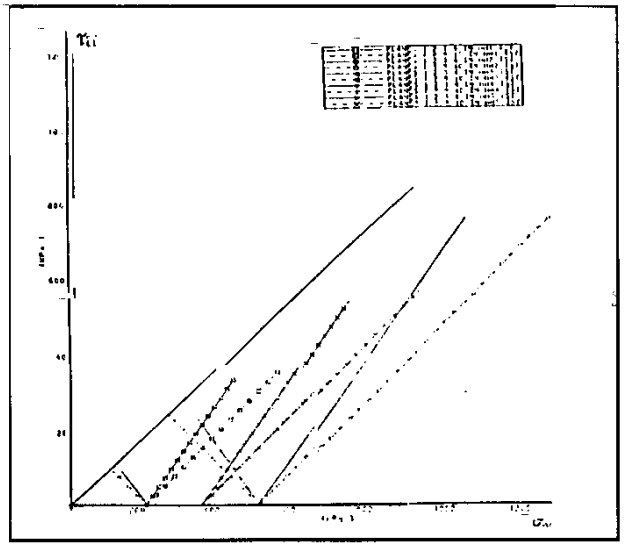

Figure.11. Stress paths correspond to active sampling planes in tests HH1. TST, HH2. TST, HH3. TST, HH4. TST, and HH5. TST

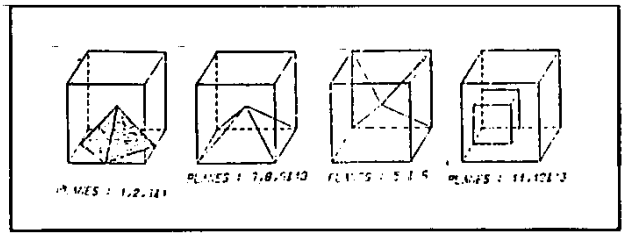

Figure. 12. The orientation of failed planes in tests: HH1. TST, HH2. TST, HH3. TST, HH4. TST, and HH5. TST

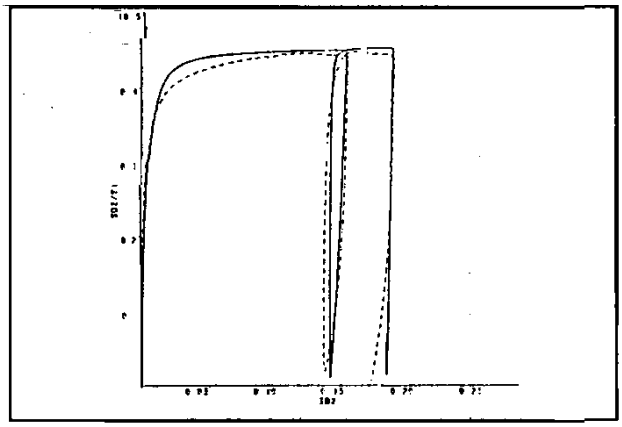

a) SD2/S1 and ID2.

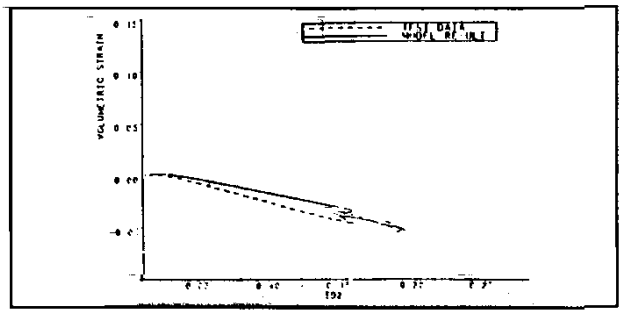

b) Volumetric strain (ε_v) ~ID2

Figure. 13. The comparison of model response with CH1. TST

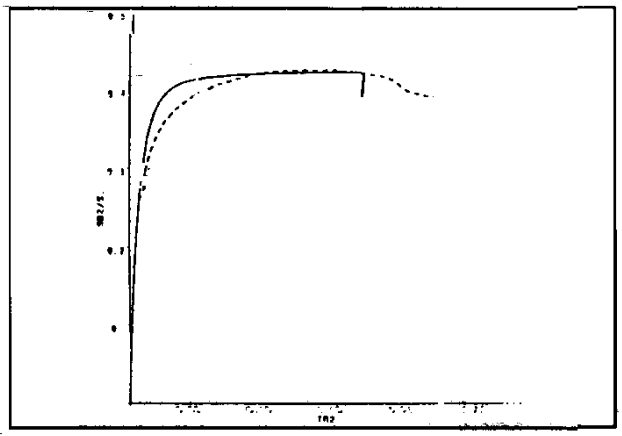

a) SD2/S1 and ID2.

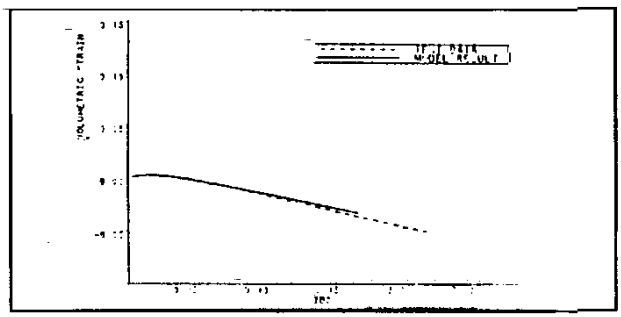

b) Volumetric strain (ε_v) ~ID2

Figure. 14. The comparison of model response with CH2. TST

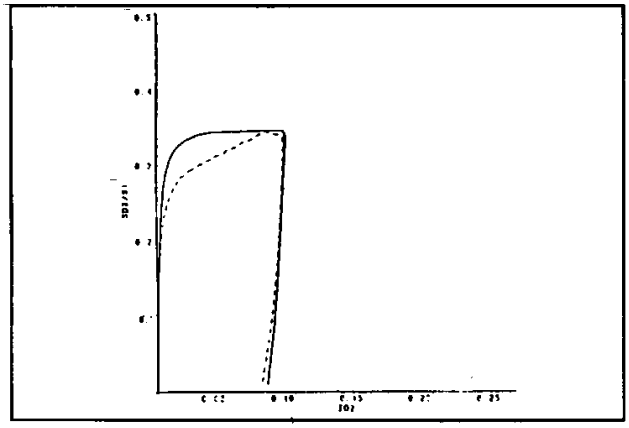

a) SD2/S1 and ID2 KPa.

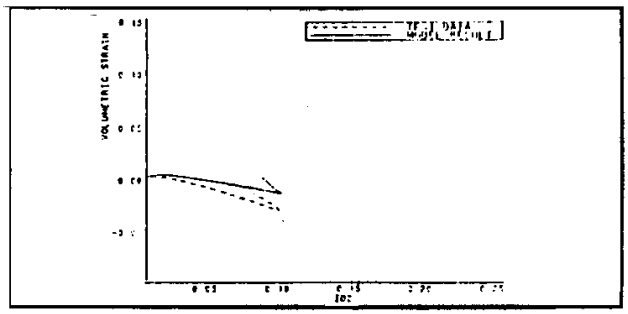

b) Volumetric strain (ε_v) ~ID2

Figure. 15. The comparison of model response with CH3. TST

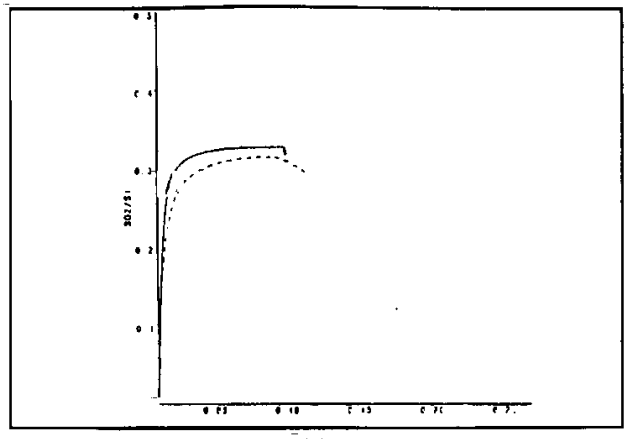

(a)

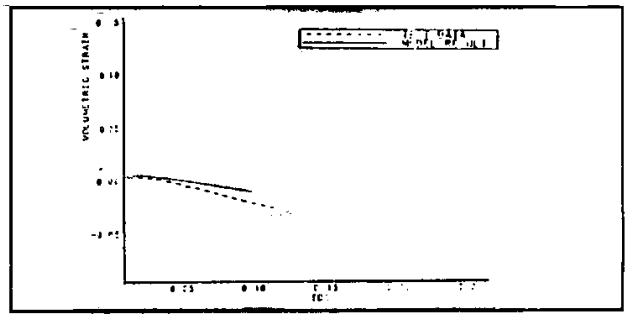

b) Volumetric strain (ε_v) ~ID2

Figure. 16. The comparison of model response with CH4. TST

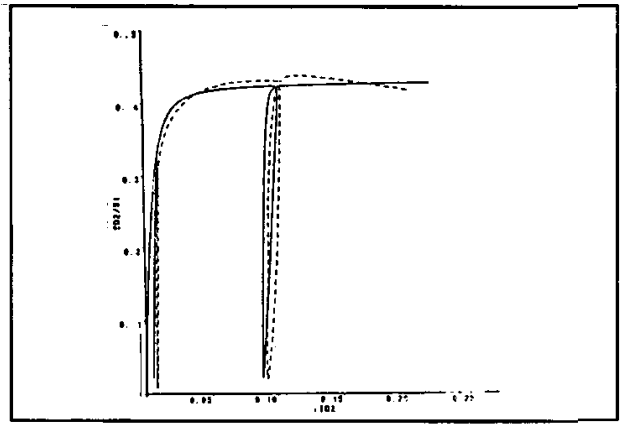

a) SD2/S1 and ID2.

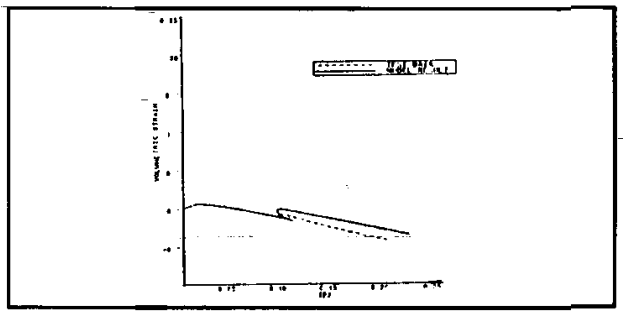

b) Volumetric strain (ε_v) ~ID2

Figure. 17. The comparison of model response with CH5. TST

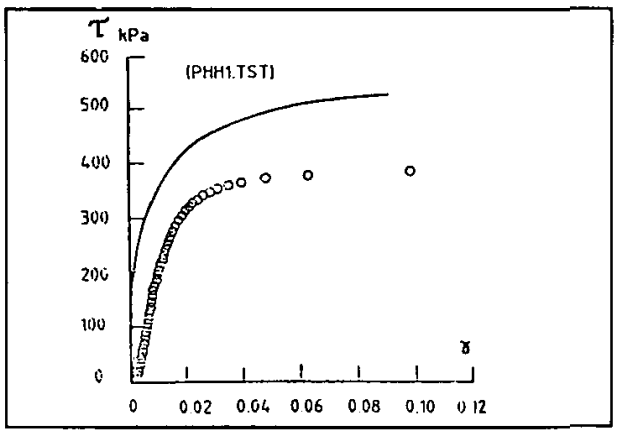

(a)

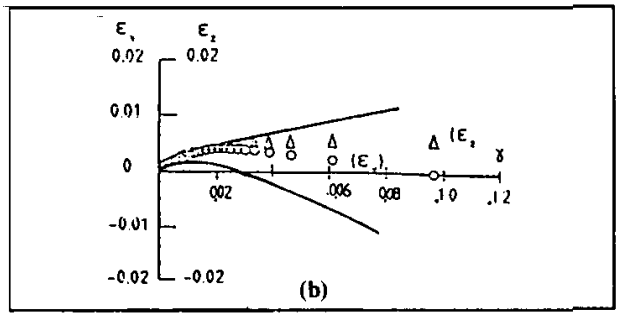

Figure 18. Results obtained for test PHH1. TST
ooooo (ε_v of model), ΔΔΔΔ (ε_z of model) and —— test

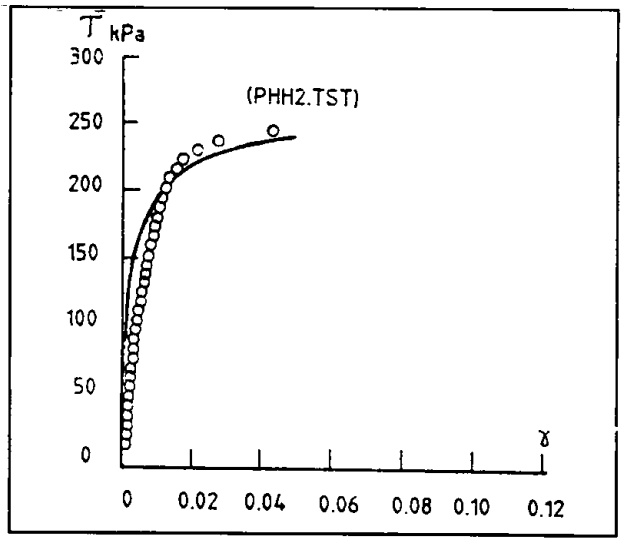

(a)

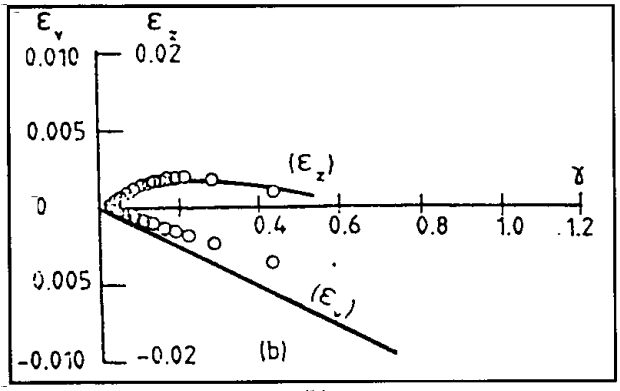

(b)

Figure. 19. Results obtained for test PHH2. TST
oooooo model and ——— test

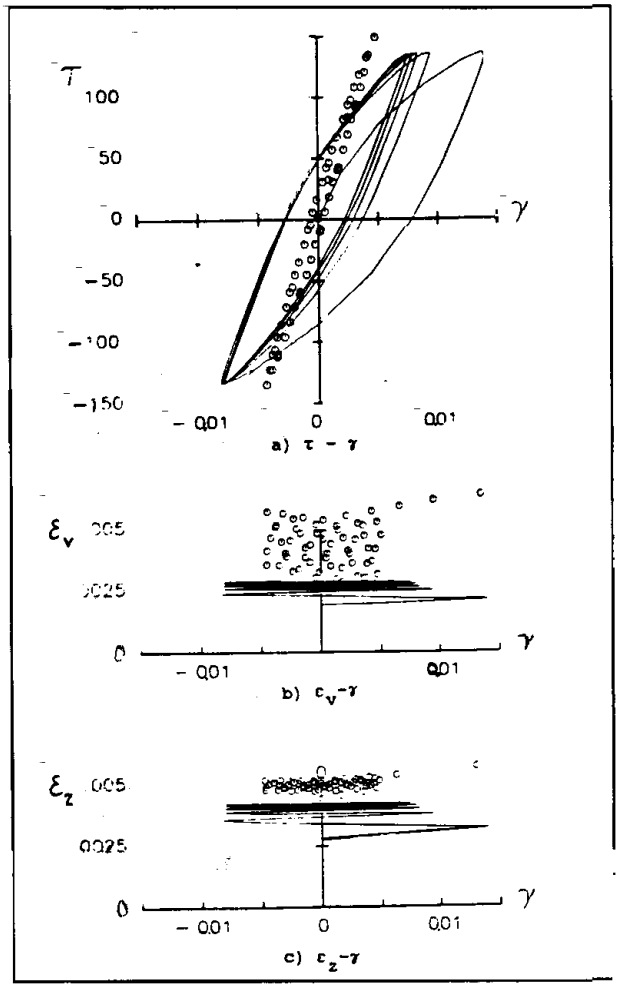

Figure. 20. Results obtained for test PHH3B. TST
oooooo model, and ——— test

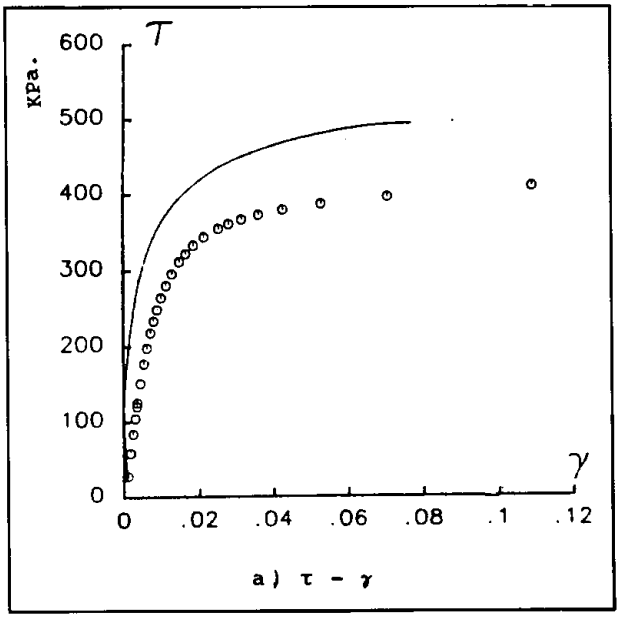

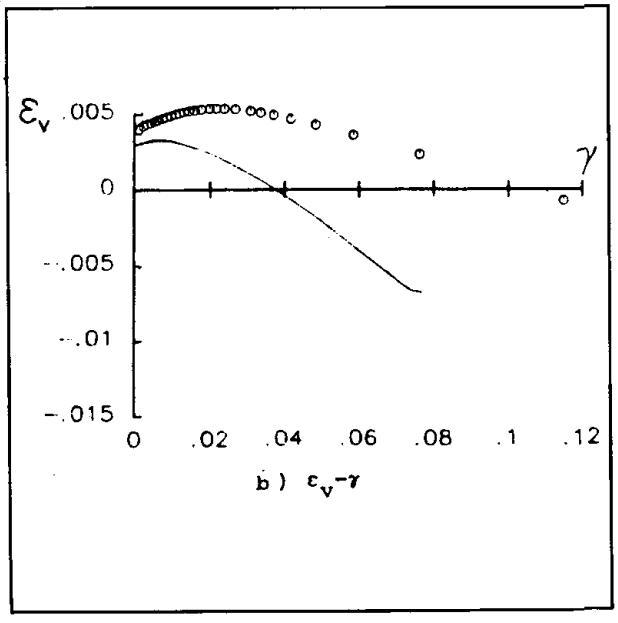

Figure 21. Results obtained for test PHH3C. TST oooooo model, and test

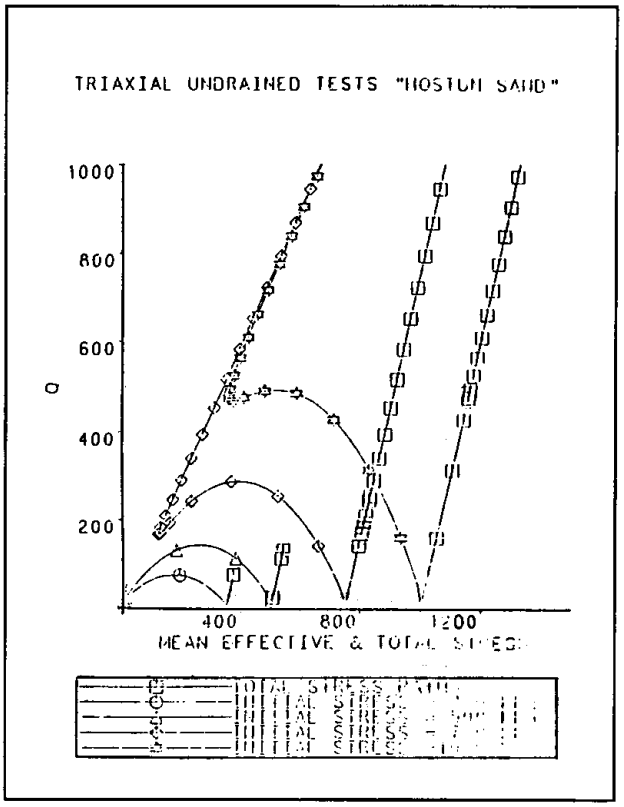

a) Effective and total stress paths for undrained compression tests.

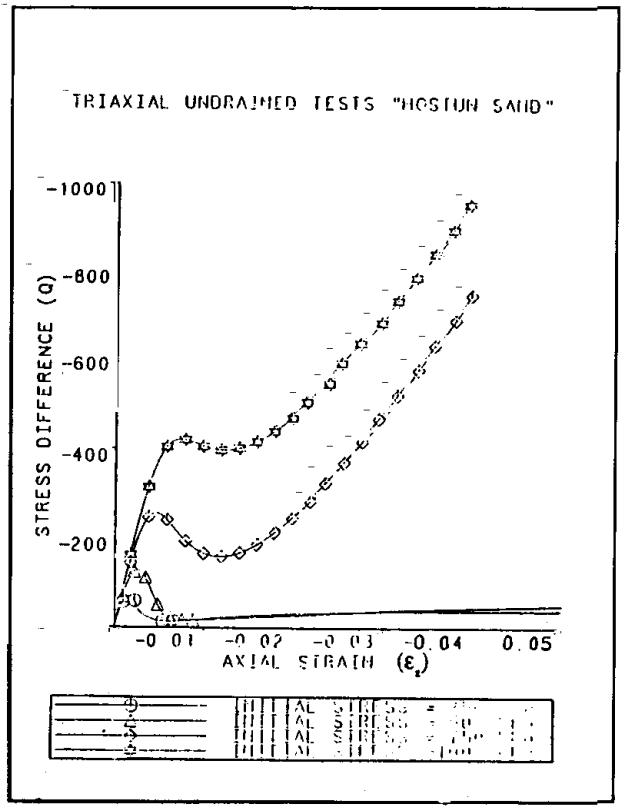

b) Variation of Q versus(ε_z)for undrained compression tests

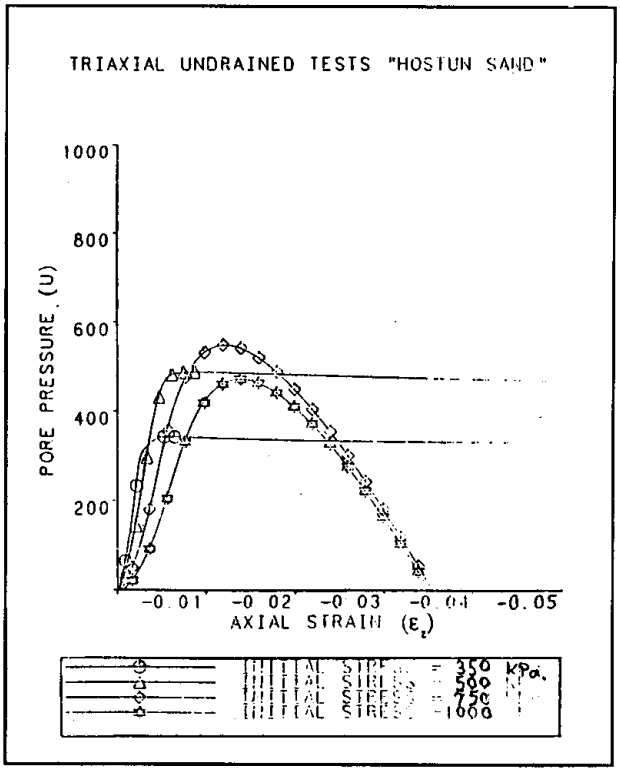

c) Variation of pore water pressure in undrained compression tests

Figure. 22

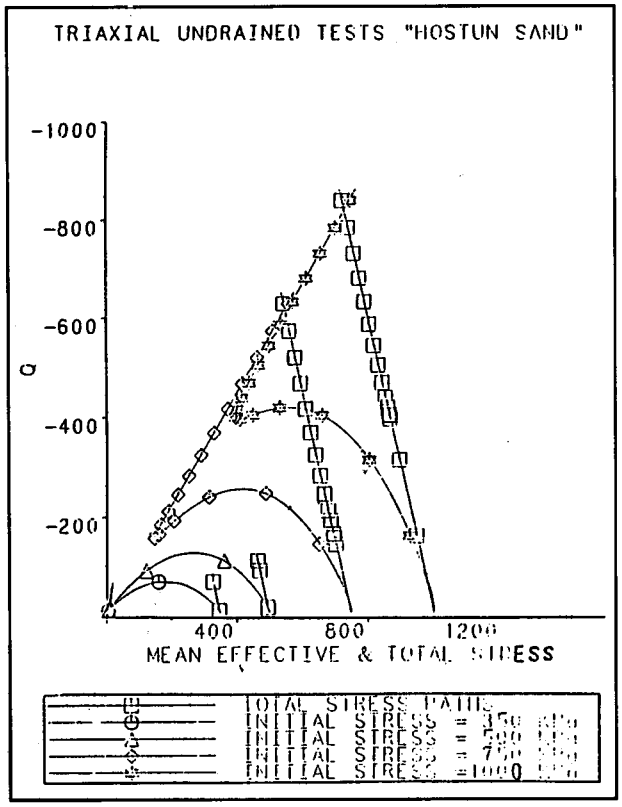

a) Effective and total stress paths for undrained extension tests

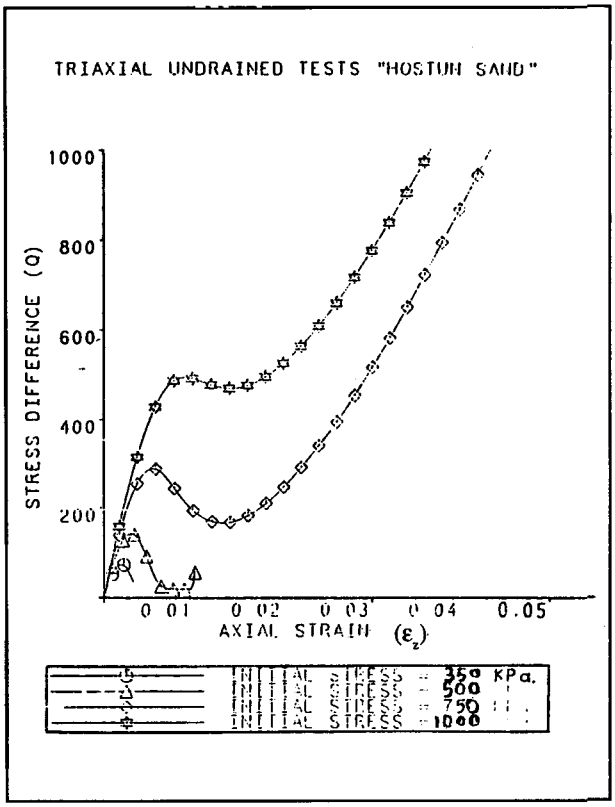

b) Variation of Q versus (ε_z) for undrained extension tests

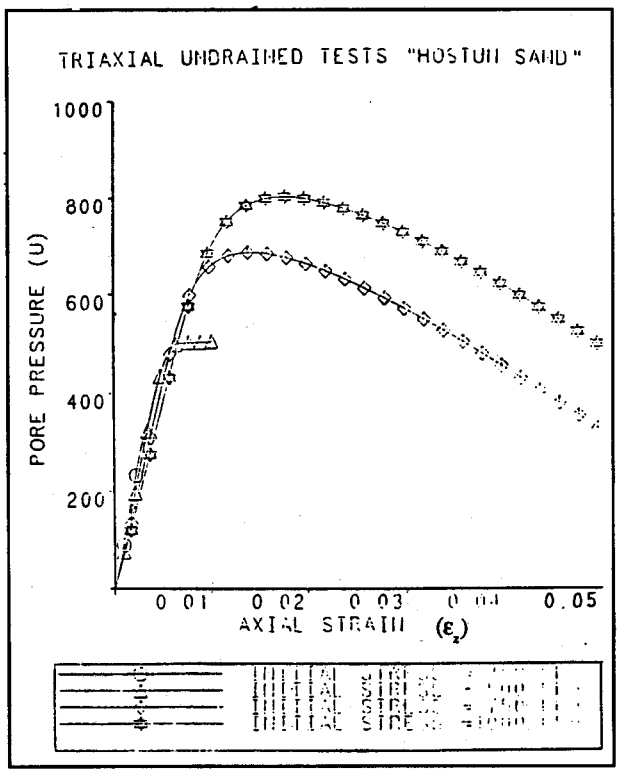

c) Variation of pore water pressure in undrained extension tests

Figure. 23